Simulation Based Density Scans On Different 2D Colodial System Configurations

Research-Oriented Project

Johannes Schumann
Friedrich-Alexander Universität Erlangen-Nürnberg
(Dated: November 7, 2018)

Dotera [1] used a step potential and gained quasicrystal phases in a colloidial system. In this project this configuration was also simulated, analysed and finally the potential was equipped with a second step. The aimed structure of this additional step was the Penrose tiling, which was used to model the distance configuration of the double-step system. In the second part of the project the DLVO potential configuration, which was used by Sandbrink [2] was tried to rebuild.

1. INTRODUCTION

Quasicrystals form an astonishing category of materials, with their structure following a well defined law of arrangement without any finite iterations with respect to its centre of rotational symmetry.
As this phenomena is already observed in many systems, the question about the reproducibility arises. In order to investigate the reproducibility, an analysis of the involved systemproperties and environment parameters is necessary.
A Monte Carlo algorithm of a certain many particle system as well as an algorithm for an automatic analysis of the tiling angles of the resulting particle distributions was developed in this work.
The analysed system configurations are mainly based on two publications. The first one is the Ph.D. thesis of Matthias Sandbrink [2], and the second one is the publication by Dotera et.al. [1], which differ by the used interaction potential (see Section 2.2).

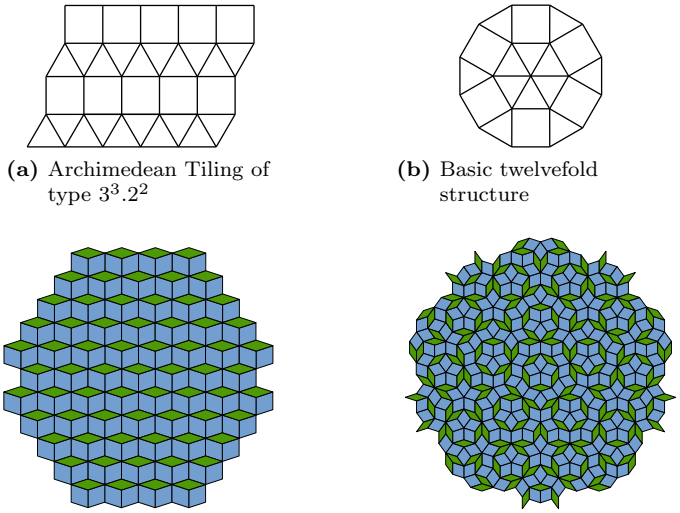

(a) Archimedean Tiling of type $3^3.2^2$

(b) Basic twelvefold structure

(c) Classical twofold symmetry tiling using the Rhombs of the Penrose tiling.

(d) Penrose tiling with tenfold symmetry.

Figure 1: Exemplary tiling structures.

2. SYSTEM PROPERTIES

The referenced many particle system represents a two-dimensional collodial NVT-ensemble.

2.1. Symmetry & Tiling Structure

The main quasicrystalline structures, considered in this work are tenfold and twelvefold symmetries. The twelvefold symmetry has a common divisor angle of $\delta = 30°$, which is connected to square or equilateral triangle[1] tiles. The basic configuration of these two tiles for a twelvefold symmetry is given in Figure 1b, whereas a larger quasicrystal grid containing it is shown in [2, Fig. 7.9c].
The most common example of tenfold symmetry is the Penrose tiling, which is shown in Figure 1d. It contains two types of rhombs, one with the long diagonal divided by the side length being equal to the golden ratio Φ^2 to the side length and one with the short diagonal divided by the side length equal to $1/\Phi$.
As it will be discussed in detail in the following Section, only radial symmetric potentials are used in this project. Thus, all tiling structures are directly related to certain lengths encoded in the interaction potential.
For both of these structures/tilings, the contained tiles can be rearranged to a classical symmetry. The square and equilateral triangles are also part of the Archimeadean tiling, shown in Figure 1a. The way to rearrange the rhombs of the Penrose tiling is shown in Figure 1c. Therefore the environment parameters are of great importance for the system to create the quasicrystaline

[1] In the following the particle structure forming equilateral triangles is just denoted as triangular tiling.

[2] Φ states the value of the golden ratio, which is: $\Phi = \frac{1+\sqrt{5}}{2} \approx 1.618$

structures, in addition to the interaction potential, to force certain angles and distance relations.

2.2. Colloid Interaction

The behaviour of the particles under certain environmental conditions is caused by the particle interaction. In this work the shoulder potential from Dotera et al. [1] and the DLVO potential from Sandbrink [2] was used. As the shoulder potential is not very similar to a real system configuration, it has major advantages in doing analysis and by encoding the length scale.
In principle, the single-shoulder potential has already two encoded lengths. It is given by

$$V(r) = \begin{cases} \infty & r < \sigma_\mathrm{C} \\ \varepsilon & \sigma_\mathrm{C} < r < \lambda\,\sigma_\mathrm{C} \\ 0 & r > \lambda\, r_\mathrm{C} \end{cases} , \tag{1}$$

where σ_C is the colloid particle diameter and λ is the length ratio compared to σ_C. The first length is the particle diameter itself, as the particles are hard and cannot intersect. The second is given through the shoulder extent, which is e.g. $\lambda = 1.4$ for the HD12 configuration. Thus, for this HD12 configuration it is expected to form square-shaped tiling for sufficient low density. For the LD10 configuration it is expected to switch to a common-divisor angle $\delta = 36°$, which is necessary for tenfold symmetry.
The publication data and the performed density scans during this project are not very promising with respect to the aimed structures (see Section 5.2). Therefore, this single-shoulder potential was equipped with a second shoulder step, meaning

$$V(r) = \begin{cases} \infty & r < \sigma_\mathrm{C} \\ \varepsilon & \sigma_\mathrm{C} < r < \lambda_1\,\sigma_\mathrm{C} \\ \tilde{\varepsilon} & \lambda_1\,\sigma_\mathrm{C} < r < \lambda_2\,\sigma_\mathrm{C} \\ 0 & r > \lambda_2\, r_\mathrm{C} \end{cases} , \tag{2}$$

where $\lambda_1 < \lambda_2$.
The second kind of potential is a DLVO[3] potential, which was also used by Sandbrink [2] (and Vogel [3]). This DLVO potential reproduces the interaction of a real colloid, including Born repulsion, Van-der-Waals attraction and electro static repulsion. The form and notation was adapted from Sandbrink, as this is the reference, which was focused on. It is composed as

$$V_\mathrm{DLVO} = V_\mathrm{Yk} + V_\mathrm{AO} \tag{3}$$

where V_YK represents the Yukawa-Potential, which describes the contribution of the electro static repulsion part including screening effects. It is given by

$$V_\mathrm{Yk} = \begin{cases} \epsilon \frac{\sigma_c}{r} \exp\left[-\kappa(r-\sigma_c)\right] & , r > \sigma_c \\ \infty & , r < \sigma_c \end{cases} , \tag{4}$$

where κ is the inverse Debye screenling length.
The other contributing effects, i.e. the potential describing these is written as

$$V_\mathrm{AO} = -\Gamma \frac{\kappa\sigma_c(1+q)^2}{\exp\left[-\kappa\sigma_c\right]} \left[1 - \frac{3r}{2(1+q)\sigma_c} + \frac{1}{2}\left(\frac{r}{(1+q)\sigma_c}\right)^3\right] , \tag{5}$$

where q is the ratio between colloid and polymer particle radius, meaning

$$q = \frac{\sigma_C}{\sigma_P} . \tag{6}$$

The parameter Γ describes the ratio between attractive and repulsive contribution to the overall potential V_DLVO [2]. In Figure 2 the functionality of the DLVO-Potential is given within a parameter scan for q with fixed Γ and vice versa.

3. SIMULATION

The Monte Carlo simulation was implemented using a standard metropolis algorithm for a many particle system. The number of Monte Carlo steps is denoted as n. With respect to the simulation setup, the used environment parameters are defined as relative variables. The temperature T is given via the parameter

$$\Theta = \frac{k_B T}{\varepsilon} , \tag{7}$$

where k_B is the Boltzman constant and ε states the order of magnitude of the used potential. It was determined with respect to a certain potential as

$$\varepsilon := \max\{r > \sigma_\mathrm{C} \ : \ V(r)\} . \tag{8}$$

The density is defined as the area fraction covered by the particles, which is

$$\rho = \frac{A_\mathrm{particle}\, N}{A_\mathrm{Box}} . \tag{9}$$

For the simulations using the DLVO potential, the density is given by

$$\eta = \frac{4\rho}{\pi}\left(1 + q^{-1}\right)^2 , \tag{10}$$

for a better comparability to the results of Sandbrink [2].
The elapsed system time τ is defined as

$$\tau = \frac{N}{n} , \tag{11}$$

which is basically the number of monte-carlo steps per particle.
The general proceeding for a simulation run was, scaning over the density ρ with the other parameters being fixed.

[3] Named after Derjaguin, Landau, Verwey and Overbeck (see [2]).

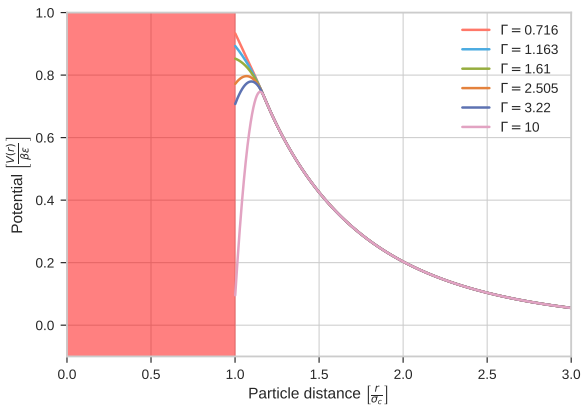

(a) Γ-parameter scan for fixed $q = 0.17$ and $\kappa\sigma_c = 0.9$.

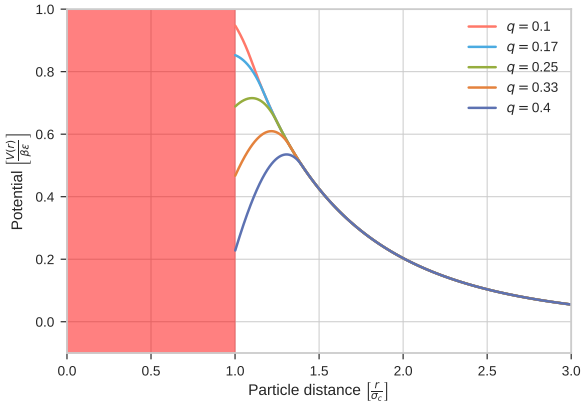

(b) q-factor scan for fixed $\Gamma = 1.61$ and $\kappa\sigma_c = 0.9$.

Figure 2: DLVO-potential-plot where the red zone shows the overleap of the colloid particles.

3.1. Simulation Box Properties

The shape of the box is not a trivial aspect, as it was investigated by Sandbrink [2, ch. 3]. Within the scope of the project, this aspect was not focused on in detail, but should not be neglected completely. In the simulation, the shape of the box is a rectangle with adjustable aspect ratio. Therefore, each configuration is simulated using two different aspect ratios, in order to get an idea of the stability of the result or possible deviations. These are a ratio of 1 (quadratic box) and one with an aspect ratio of the golden ratio Φ. The boundaries of the box are simulated as periodic boundaries. The dimension of the box was chosen related to the amount of particles, which was aimed to be around $N \approx 800$.

3.2. Initial Particle Placement

It is very likely, that the system provides multiple local minima with respect to the system energy. Thus, the initial placement of the particles plays an important role in which minimum the system will terminate at equilibrium.
A distribution of randomly placed particles is likely the most intuitive initial configuration, because it has no preferred tiling. Thus, this random particle arrangement is the main one used and is tested for each system configuration.
It gets very complex to place the particles completely random without causing overlaps at high densitys. Therefore, the positions are not checked for overlaps while placing them. For solving this violation of the constraint of hard particles, a "curing" process is introduced. Technically this is realized by modifing the input potential $V(r)$ to

$$\tilde{V}(r) = \begin{cases} V(\sigma_\mathrm{C}) - c\,n\,(\sigma_\mathrm{C} - r), & r < \sigma_\mathrm{C} \wedge n \leq 10^4 \\ \infty, & r < \sigma_\mathrm{C} \wedge n > 10^4 \\ V(r), & r > \sigma_\mathrm{C} \end{cases} . \tag{12}$$

In general, $V(r)$ should be infinity for $r < \sigma_\mathrm{C}$, in order to reject a MC step when it comes to an overlap. With the modified potential, the slope of the edge at $r = \sigma_\mathrm{C}$ is increasing with n, which is called "curing" here.
In order to test the stability, specific tilings are also used as initial arrangement. This is done if a certain geometry is expected for a certain configuration, e.g. Penrose tiling or square tiling.

4. ANALYSIS

The analysis part requires an algorithm to categorise a given particle distribution regarding its tiling. This is done via the ocurring angles between the connection lines to the neighbours of every particle. To determine these, the following algortihm is applied on the results:

1. The unit cell tiling for a given particle distribution is determined using the Voronoi algorithm.
2. The unit cells are investigated for geometric degeneracies. These turn out to unit cell angles, which are not well distinct, but flattend by an additional short edge. Therefore all edges of the unit cells with a length less than r_C are removed.
3. The angles between the center of the unit cell and two neighbouring points, which span connected edges of the unit cells are calculated (see Figure 3).

(4.) Based on the angle distribution, the number of tiles for each identifiable type is calculated.

The developed analysis implementation displays the results of steps 1-3 as an angle histogram.
For verifying the simulation implementation and the analysis procedure, it was first tested on configurations of previously well known systems. These two configurations are `HD12` and `LD10` of Dotera [1], of which the results can

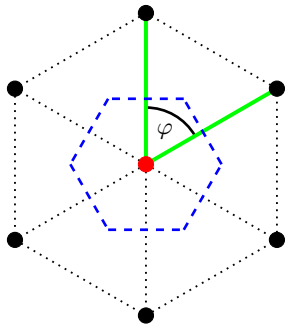

Figure 3: Unit cell (blue) for a regular threefold tiling. The angle φ is spanned by connection lines (green) to the neighbouring points. These are perpendicular to connected ridges of the unit cell.

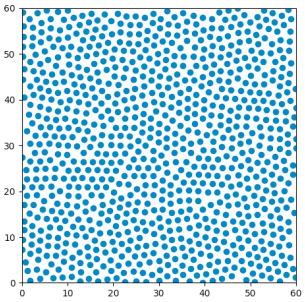

(a) HD12 Particle distribution.

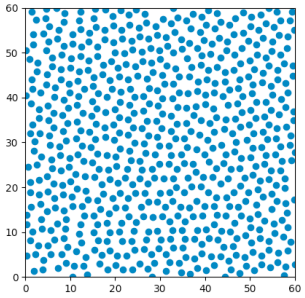

(b) LD10 Particle distribution.

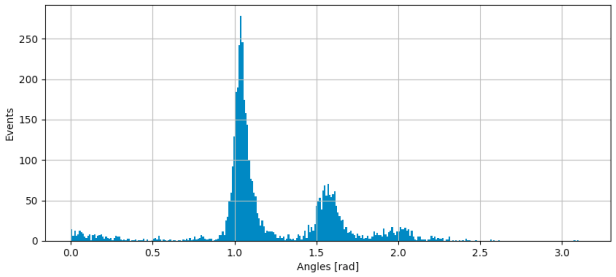

(c) HD12 Angle distribution.

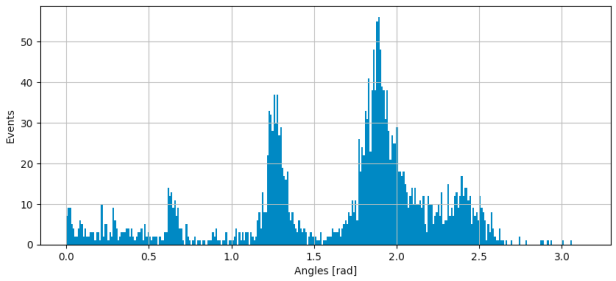

(d) LD10 Angle distribution.

Figure 4: Simulated configuration HD12 according to the descriptions of Dotera et al. [1] with randomly placed particles after $\tau = 4.5 \times 10^5$. As it is expected, the peaks are at multiples of the common divisor angle ($\delta_{\mathrm{HD12}} = \frac{\pi}{6}$ and $\delta_{\mathrm{LD10}} = \frac{\pi}{5}$).

be seen in Figure 4. The results show for a specific tiling, the angles condensate at the multiplices of the common divisor angle δ. Therefore, the fourth step of the algorithm is done by fitting a predefined angle distribution function to the histogram. If this step is applied in the following, the angle distribution function is composed of multiple Gaussians, meaning

$$f(\varphi) = \sum_{k=1} A_k \exp\left(-\frac{\varphi_k^2}{2\,\sigma_k}\right) \quad . \tag{13}$$

The area within the FWHM of a single Gaussian over the bin width gives the number of edges with angle φ_k.
In scope of this project, no particles where tracked while the Monte Carlo steps are applied. Thus, there is no differentiation between fluid and unordered solid phases. In following these are denoted as fluid and are identified in the angle-density profile by missing significant peaks at certain angle values.

5. RESULTS & DISCUSSION

5.1. DLVO Potential

The first system, which was analysed using the specified algorithm in the previous Section, is the configurations used by Sandbrink [2] based on the DLVO potential. As there is an expected result from his Ph.D. thesis available, this can be used as starting point regarding the parameter configuration[4] for $\eta, \Gamma, \kappa\sigma_c, \epsilon\beta$ and q.
Figure 5a shows an overview of the tiling structures to expect at $\Gamma = 1.61$ and $q = 0.17$. The results for a density scan at $\epsilon\beta = 80$ are shown in Figure 5b and 5c These results just show a triangular tiling in the solid phase as the dominant angle in the whole structure is at $\frac{\pi}{3}$. This behaviour might be caused by the potential functionality shown in Figure 2, which is repulsive over all particle distances for $\Gamma = 1.61$ and $q = 0.17$.
It is very complex to estimate a certain tiling for this pure repulsive potential configuration, as there is no obvious length-scale existing. So the accordance to the tiling-structure map in Figure 5a could not be verified. In Figure 12 the resulting tilings are shown, which the angle-density profile in Figure 5b is based on. There, most of the occuring structures can be identified with triangles.
After detailed investigation of the software implementation and parameter interpretation no major error was found.
Therefore, it was tried to scan the parameters Γ and q at some fixed configuration, where no triangular tiling is expected. The chosen configuration is $\beta\epsilon = 80$ and $\eta = 1.3$, which should produce a fourfold tiling according to Figure 5a. Due to limited computation time not

[4] For this system the notation differs from the definition in Equation (7), where it is denoted as $\beta\epsilon = \Theta^{-1}$.

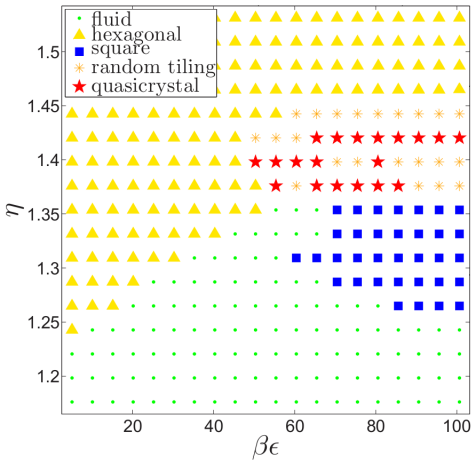

(a) Expected tiling structures over the system temperature and density η according to Sandbrink. Figure taken from [2].

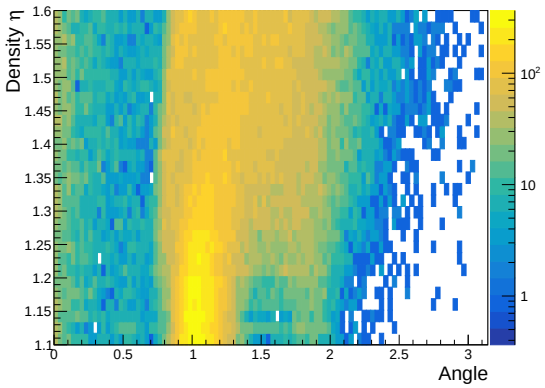

(b) Angluar distribution for $\beta\epsilon = 80$ and initialized with random placed particles.

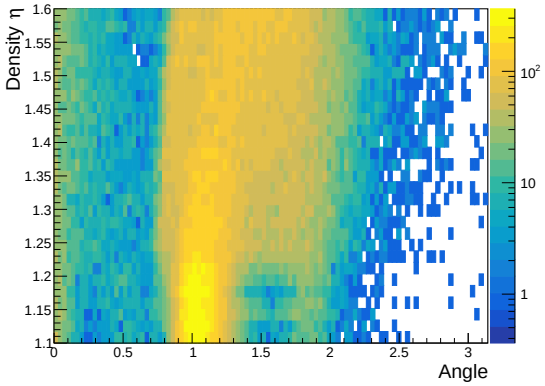

(c) Angluar distribution for $\beta\epsilon = 80$ and initialized with a rectangular tiling.

Figure 5: Results for the DLVO potential

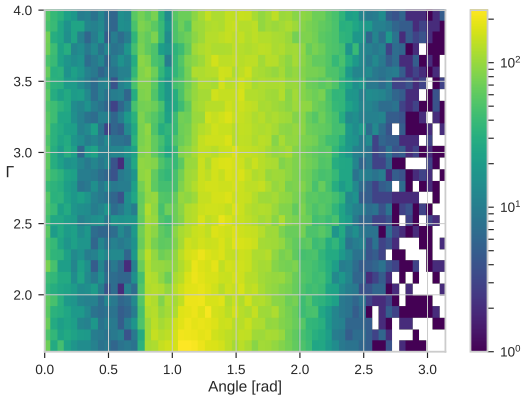

(a) Γ scan

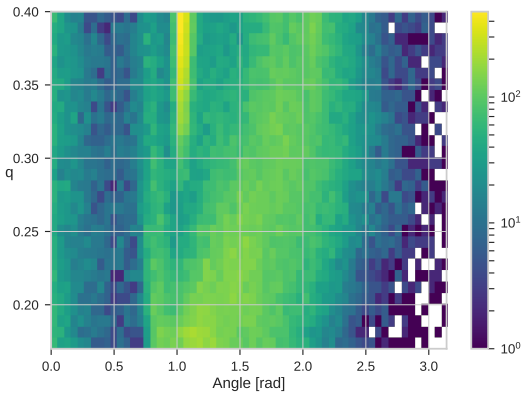

(b) q scan

Figure 6: Parameter q, Γ scan for the DLVO systems for configuration used by Sandbrink [2]

the whole plane spanned by the parameters Γ, q was scanned. Instead, only one parameter was varied where the other one was fixed at the initial configuration value ($\Gamma = 1.61$, $q = 0.17$). The limits of the scan were chosen with respect to the physical properties of a real system, which limits the maximum size of the substrate particles and the attraction-repulsion ratio. These ranges were chosen as

$$q \in [0.17, 0.4] \tag{14}$$

and

$$\Gamma \in [1.61, 4] \ . \tag{15}$$

The results of the scans are shown in Figure 6. In the distribution resulting from the Γ scan (see Figure 6a) no dominant peak appears at a certain angle value. For the q scan (see Figure 6b) such a peak appears for $q > 0.32$, which is at $\frac{\pi}{3}$ and indicates threefold symmetry. Due to the limited project time this system was not further investigated.

5.2. Single-Step Potential

The second kind of potential, which was studied is the single-step potential (see Equation (1)), which was used by Dotera et al. [1]. The considered configurations are HD12 and LD10, which were scanned over a density range of $\rho \in [0.1, 0.9]$. There are two points of interest for rebuilding this system, which are the general reproducability and the accordance of the angle-density profile to the expected crystal phases, which are shown in Figure 7. The resulting angle-density profiles of the done simulations are shown in Figure 8. Comparing the profiles of each configuration with respect to the used box aspect ratios, there are obviously no major differences (see Appendix - Figure 16).

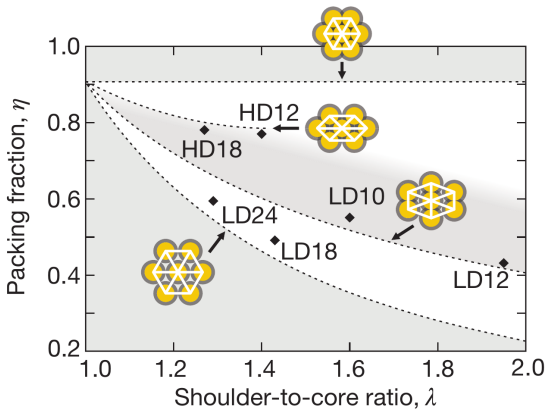

Figure 7: Expected tiling structures over the parameter λ and density ρ according to Dotera et al. [1]. Figure taken from [1, Fig. 1d].

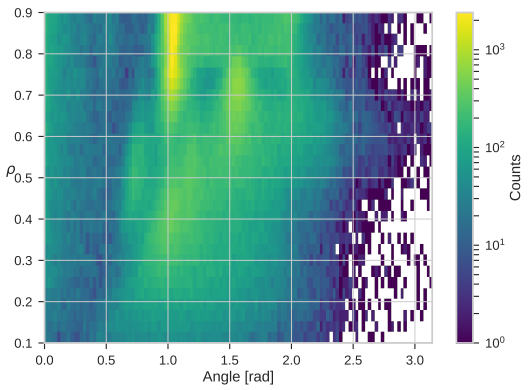

(a) HD12, box size (60, 60)

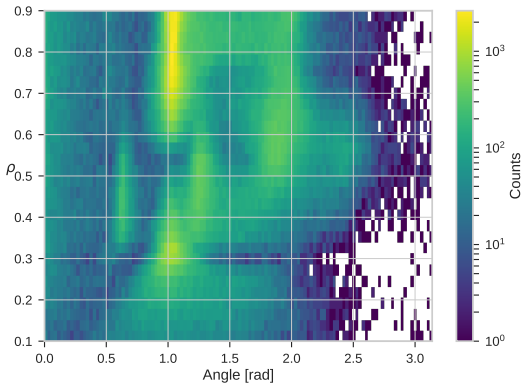

(b) LD10, box size (60, 60)

Figure 8: Angle-density profile for an angular scan of the configurations LD10 and HD12, defined by Dotera et al. [1]. The results are shown for the squared aspect ratio of the system container. The results for both aspect ratios of the system container are given in the Appendix in Figure 16.

The HD12 configuration has a $\lambda = 1.4$, which is gives the side-diagonal ratio of a square. Thus, it is expected to gain a certain fraction of square tiles using this configuration. Based on the applied angle analysis the angle-density profile (see Figure 9a) indicates square tiles between $\rho \in [0.68, 0.8]$, which can be seen through the ridge at $\frac{\pi}{2}$. In Figure 10 the HD12 angle-density profile is converted to a corresponding number of square and equilateral triangle tiles. The figure shows also the densities for different ideal structures, which can be formed by a system with a common divisor angle of $\delta = \frac{\pi}{3}$, e.g. pure equilateral triangular, square, Archemedean and twelvefold tiling.

In this representation it can be seen, that the number of triangular tiles dominates the density range where the densities of square, twelvefold and Archimedean tiling are located at. The number of triangles drops attending lower densities at $\rho \in [0.7, 0.75]$, which does not result in a significant increase of square tiles. An exemplary tiling result within the density range $\rho \in [0.68, 0.8]$ is given in Figure 9a. The gathered structure has apparently no long-range order, just local patches of triangle and square tiling.

A very similar behaviour was observed for the LD10 configuration, which flips to the quasicrystalline phase indicated by a common divisor angle of $\delta = \frac{\pi}{5}$ roughly in $\rho \in [0.45, 0.57]$. The exemplary tiling for this quasicrystal phase of the LD10 configuration is given in Figure 9b at $\rho = 0.52$. Even though the particles form a structure with the aimed common divisor angle, the dominant patterns are particle chains rather than certain repetitive tiles forming a global structure. Around $\rho = 0.3$ the LD10 configuration flips again to a triangular structure, which can be explained by the estimation of Equation (18). At lower densities the well defined peaks in the angle-density profile start to disappear for both systems and the configurations show a transition over to the fluid phase. The flip occuring at a lower density than for HD12 can be explained by the higher inner pressure, which is caused by the higher step distance coverage.

These oberservations agree with the results of Dotera [1] comparing it to Figure 7.

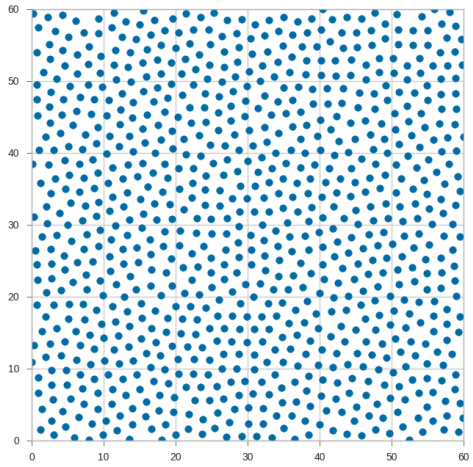

(a) HD12, $\rho = 0.76$

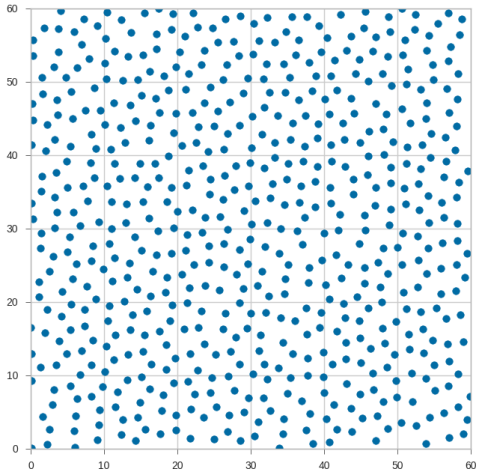

(b) LD10, $\rho = 0.52$

Figure 9: Resulting tiling structurs of LD10 and HD12 at in the indicated quasicrystalline phase by the angular-density profile. (Exemplary tilings for all phases are given in Appendix Figure 13 and 14.)

5.3. Double-Step Potential

The idea of using a second step in the potential is induced by the results of the single-step potential, where the structures a not very distinct. Also the density range for the needed properties forming desired structures is not very broad. Furthermore, in order to form a Penrose tiling, which is shown in Figure 1d, a third length-scale has to be encoded to the potential.
The two rhombe types of the Penrose tiling have the golden ratio and the golden ratio squared as their specific lengths (besides the minimal particle distance), which have to be encoded into the potential by setting the $\lambda_{1,2}$ parameters to

$$\lambda_1 = \Phi \tag{16}$$
$$\lambda_2 = \Phi^2 \ . \tag{17}$$

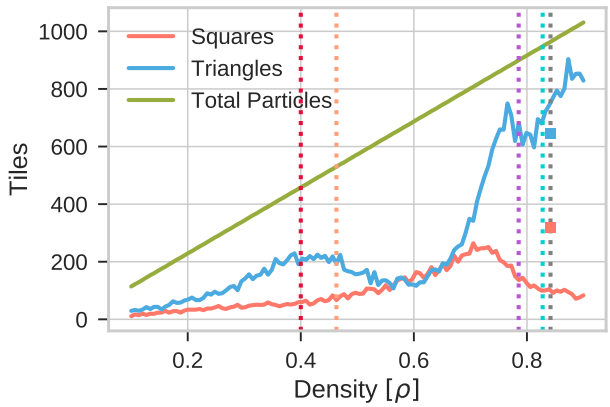

Figure 10: Number of equilateral triangle and square tiles compared to the total particle number and the density of different tiling structures. The vertical lines show these densities for: the Archemedean tiling $3^3.2^2$ (see Figure 1a) (grey), the twelvefold patch (see Figure 1b) (turquoise), the square tiling (violet), the triangular tiling with side length $a = \lambda$ (orange) and the square tiling with side length $a = \lambda$ (red). The squares on the Archemedean density line (grey) show the expected amount of triangles and squares for that distribution.

As this double-step potential system is not based on previous analysis results, no expected tiling behaviour with respect to the density ρ of the colloid is given. A perfect Penrose tiling has a density of $\rho_{\text{Penrose}} = 0.8$ and particles forming decagons with side length of σ_c have a density of $\rho_{\text{Decagon}} = 0.51$. Other expectations regarding the tiling behaviour can be derived from the potential. The maximal density for $\langle r \rangle > \lambda_1$ and $\langle r \rangle > \lambda_2$ is given by

$$\tilde{\rho}_1 = \frac{\rho_\Delta}{\lambda_1^2} = \frac{0.91}{\Phi^2} = 0.347 \quad \text{and} \tag{18}$$
$$\tilde{\rho}_2 = \frac{\rho_\Delta}{\lambda_2^2} = \frac{0.91}{\Phi^4} = 0.133 \ , \tag{19}$$

where ρ_Δ is the density for a triangular tiling. The parameters Θ, ρ and the ratio $\varepsilon_1/\varepsilon_2$ (where $\varepsilon_1 = 1$) are the (remaining) free parameters. As this potential is very close to the LD10 configuration [1], the temperature parameter was applied with

$$\Theta = 0.133 \tag{20}$$

For each run the density was varied between $\rho \in [0.1, 0.9]$, where the values for the ratio $\varepsilon_1/\varepsilon_2$ were in

$$\varepsilon_1/\varepsilon_2 \in \{0.1, 0.15, 0.18, 0.2, 0.25, 0.5, 0.75\} \ . \tag{21}$$

The angle-density profile for a varied density is shown in Figure 11 for $\varepsilon_1/\varepsilon_2 = 0.25$. It turned out that this distribution is equal for all tested values for $\varepsilon_1/\varepsilon_2$ (where

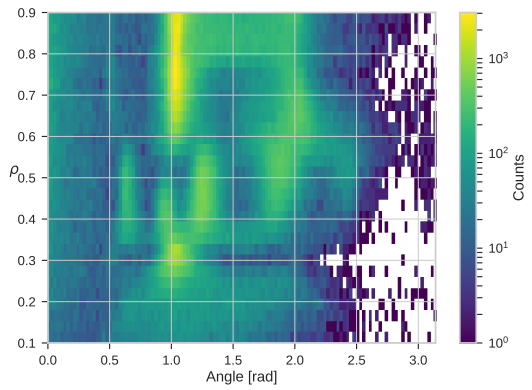

(a) Box size $(60, 60)$

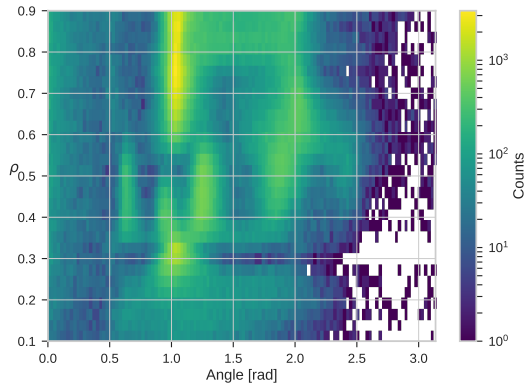

(b) Box size $(80, 50)$

Figure 11: Angle-density profile over the particle density for the configuration $\Theta = 0.133$, $\lambda_1 = \Phi$, $\lambda_2 = \Phi^2$ and $\tau = 6.5 \cdot 10^5$ (and $\varepsilon_1/\varepsilon_2 = 0.25$). The actual tilings results are exemplarily given at six densities in the appendix in Figure 15.

$\varepsilon_1 < \varepsilon_2$).
The resulting angle-density profile can be split up into four density regions with respect to the angular distibution. In between $\rho \in [0.6, 0.9]$ the threefold tiling dominates, which is indicated by the peak at $\frac{\pi}{3} (\equiv 60°)$. For descreasing density within this region a second ridge at $\frac{2\pi}{3}$ $(\equiv 120°)$ gets evident. This ridge is caused by hexagons in the tiling and can also be seen in the actual structure (see Figure 15g). As the distance of the opposite particles in those hexagons is $r > \lambda_2$, this is the energetic most favourably structure.
The second region $\rho \in [0.34, 0.6]$ is the quasicrystal phase, the common divisor angle being $\delta = 36°$. Even though, the density of the Penrose tiling is not in the density range of this phase, the density for decagons structures ρ_{Decagon} is.
The transition from the quasi-crystalic phase to the third region is exactly where it was expected by $\rho = \tilde{\rho}_1$, where the particles form again a triangular phase. This phase is located in $\rho \in [0.25, 0.34]$. The triangular tiling, being the most dense structure, is formed to gain a particle distance $r > \lambda_1$ and avoid a contribution to the system energy of the higher potential step. The last phase is the fluid phase $\rho \in [0.1, 0.25]$, which covers a higher density range, than it is expected. The difference of the transition point compared to $\tilde{\rho}_2$ can be explained by the system temperature.

6. CONCLUSION & OUTLOOK

The most promising results of this project were achieved using the double-step potential. Even though these results did not lead to a perfect Penrose tiling, the gained particle distribution shows a very prominent partial tenfold symmetry. It is indicated by a common divisor angle of $\delta = \frac{\pi}{5}$ in the angular distibution (see Figure 11) and can be seen very prominently in the particle distribution in Figure 15d.
The results of the density scan for the single step potential are in accordance with the results of Dotera [1]. The results based on the DLVO potential, which were based on the results of Sandbrink [2], could not be reproduced. The most evident explenation are differences in the system configuration, which were caused by As so far, the gained results were not classified with respect to the errors. In order to gain completely non-correlated results, the simulation runs have to be redone, which requires high computation resources. An idea to bypass this problem is, to sample the results of a single simulation-run at different time-steps τ. As these samples are correlated, this has to be considered for calculating these errors.
The simulation implementation can be retrieved from `https://www.github.com/8me/QuasiCrystal_MC`.

[1] T. Dotera, T. Oshiro, and P. Ziherl. Mosaic two-lengthscale quasicrystals. *Nature*, 506:208 EP –, 02 2014. URL: `http://dx.doi.org/10.1038/nature12938`.
[2] Matthias Sandbrink. *Tailored Colloidal Quasicrystals*. PhD thesis, Heinrich-Heine-Universität Düsseldorf, Dec. 2014.
[3] Nicolas Vogel, Clemens K. Weiss, and Katharina Landfester. From soft to hard: the generation of functional and complex colloidal monolayers for nanolithography. *Soft Matter*, 8:4044–4061, 2012. URL: `http://dx.doi.org/10.1039/C1SM06650A`, `doi:10.1039/C1SM06650A`.

Acknowledgments

This study was done within a research oriented project at the department of theoretical physics in the group of Prof. Schmiedeberg.

Appendix A: Simulation Run Details

Configuration	Θ	τ	η, ρ	Box size
DLVO	1.25×10^{-2}	10^5	$\eta \in [1.1, 1.6]$	(60,60)
HD12	0.278	10^5	$\rho \in [0.45, 0.9]$	(60,60)
HD12	0.278	10^5	$\rho \in [0.45, 0.9]$	(80,50)
LD10	0.133	10^5	$\rho \in [0.45, 0.9]$	(60,60)
LD10	0.133	10^5	$\rho \in [0.45, 0.9]$	(80,50)
Double-Step	0.133	10^5	$\rho \in [0.45, 0.9]$	(60,60)
Double-Step	0.133	10^5	$\rho \in [0.45, 0.9]$	(80,50)

Table I: Overview of the used environmental parameters in the simulations.

Appendix B: Additional Figures

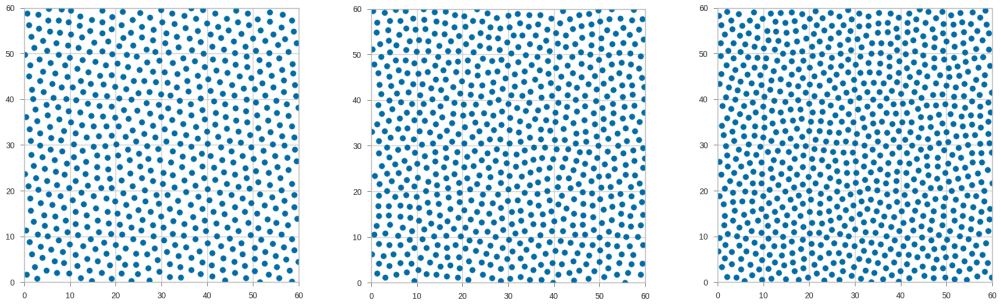

(a) $\eta = 0.92$ **(b)** $\eta = 1.05$ **(c)** $\eta = 1.18$

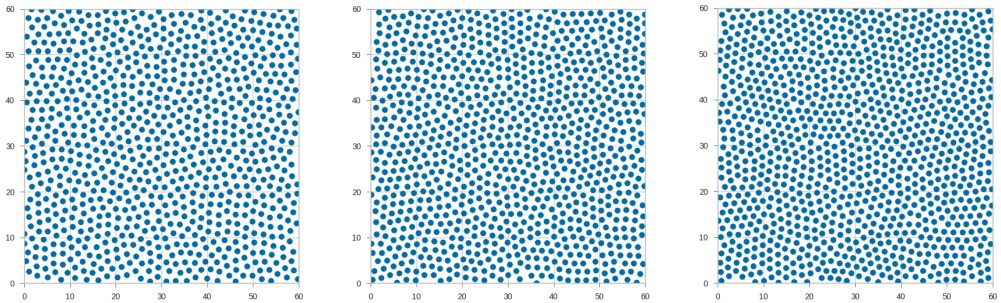

(d) $\eta = 1.32$ **(e)** $\eta = 1.45$ **(f)** $\eta = 1.57$

Figure 12: Resulting tiling structures for the DLVO configuration with square box shape.

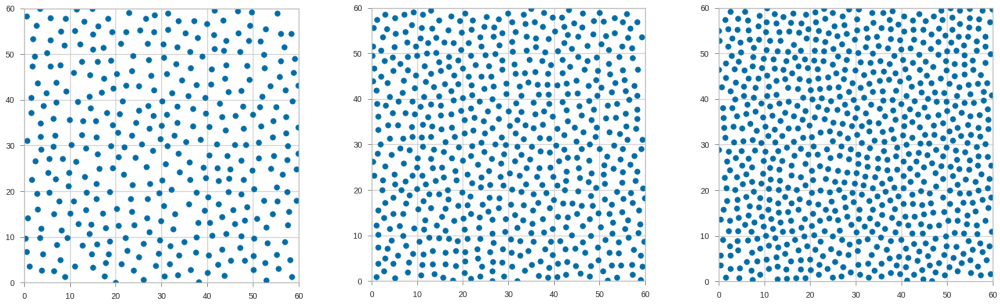

(a) $\rho = 0.3$ (Phase: Fluid) **(b)** $\rho = 0.5$ (Phase: Fluid) **(c)** $\rho = 0.63$ (Phase: QC, Fluid)

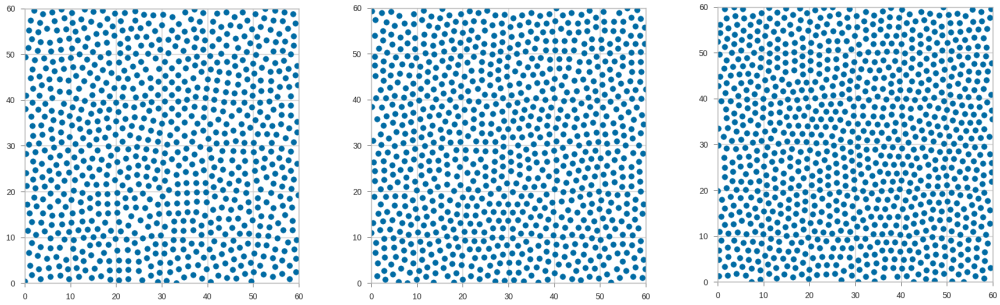

(d) $\rho = 0.71$ (Phase: QC) **(e)** $\rho = 0.76$ (Phase: QC) **(f)** $\rho = 0.83$ (Phase: Triangular)

Figure 13: Resulting tiling structures for HD12 with square box shape. For tilings at densities close to the transition between two phases, both are declared.

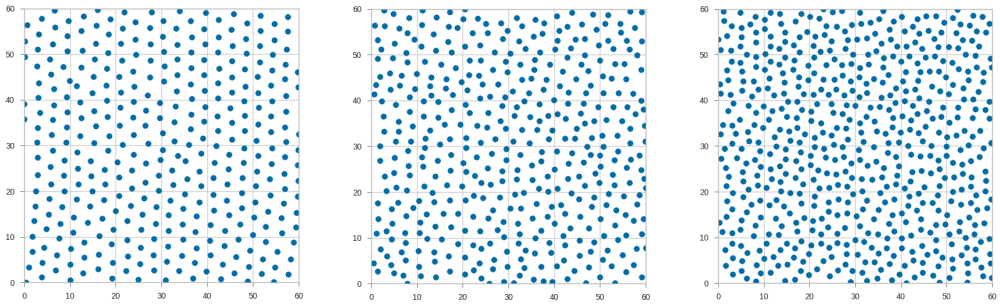

(a) $\rho = 0.3$ (Phase: Triangular LD) **(b)** $\rho = 0.36$ (Phase: QC, Triangular LD) **(c)** $\rho = 0.5$ (Phase: QC)

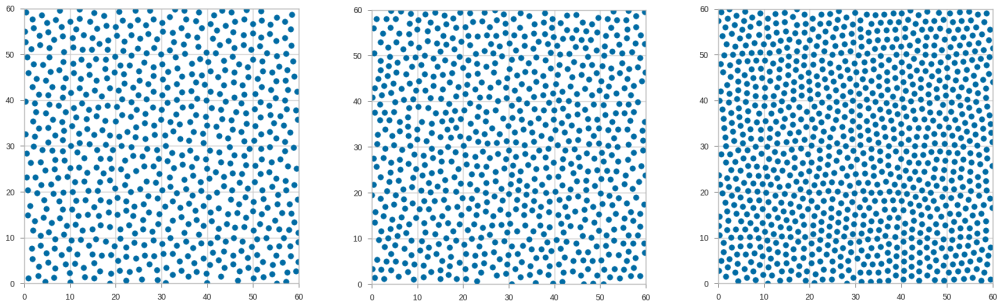

(d) $\rho = 0.57$ (Phase: Triangular HD, QC) **(e)** $\rho = 0.63$ (Phase: Triangular HD) **(f)** $\rho = 0.83$ (Phase: Triangular HD)

Figure 14: Resulting tiling structures for LD10 configuration with square box shape. For tilings at densities close to the transition between two phases, both are declared.

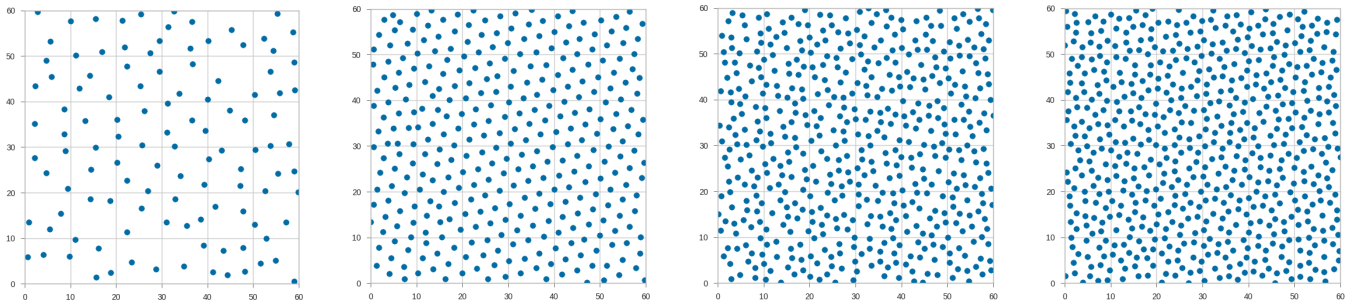

(a) $\rho = 0.1$ (Phase: Fluid) **(b)** $\rho = 0.53$ (Phase: Triangular LD) **(c)** $\rho = 0.45$ (Phase: QC) **(d)** $\rho = 0.53$ (Phase: QC)

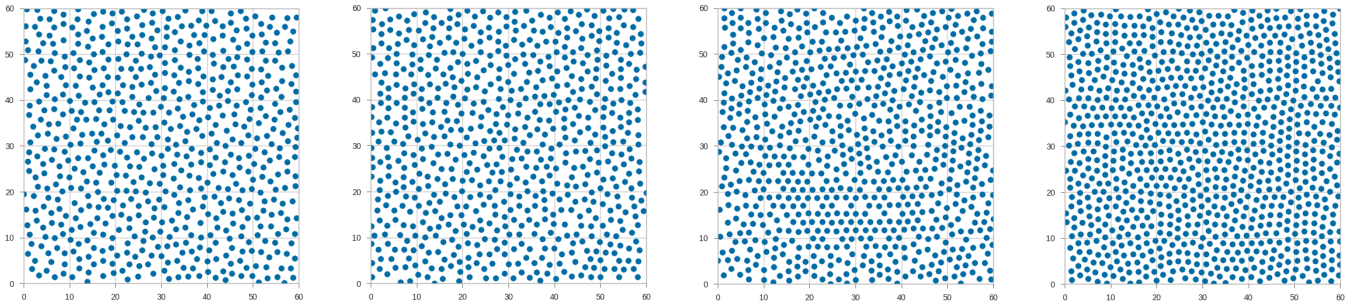

(e) $\rho = 0.56$ (Phase: QC) **(f)** $\rho = 0.6$ (Phase: Triangular HD, QC) **(g)** $\rho = 0.67$ (Phase: Triangular HD) **(h)** $\rho = 0.8$ (Phase: Triangular HD)

Figure 15: Resulting tiling structures for the double-step potential with square box shape. For tilings at densities close to the transition between two phases, both are declared.

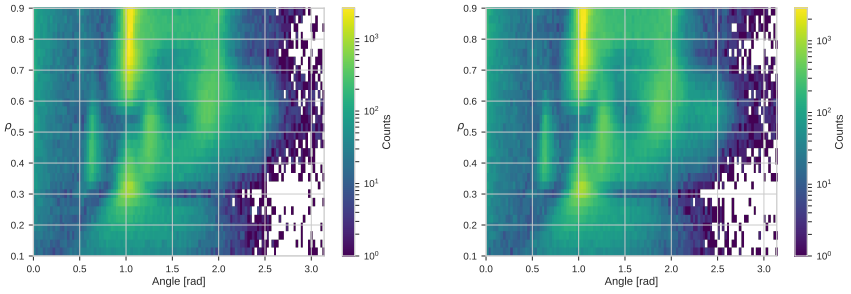

(a) LD10, box size (60, 60) **(b)** LD10, box size (80, 50)

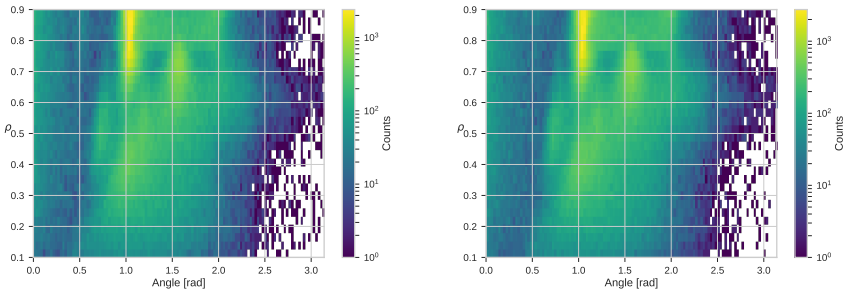

(c) HD12, box size (60, 60) **(d)** HD12, box size (80, 50)

Figure 16: Angular distribution for an angular scan of the configurations LD10 and HD12, defined by Dotera et al. [1]. For tilings at densities close to the transition between two phases, both are declared.